Journal of Materials Chemistry A

Accepted Manuscript

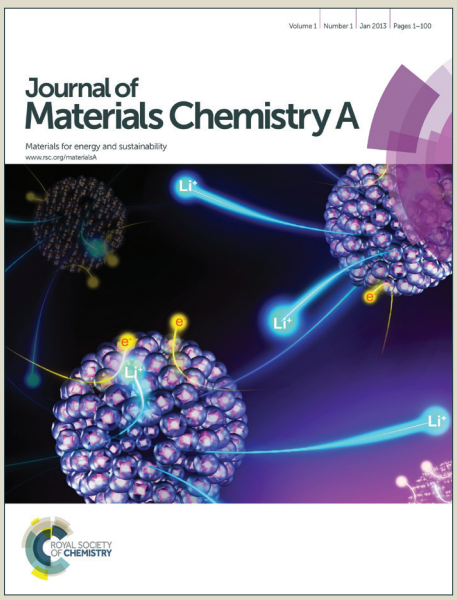

ROYAL SOCIETY OF CHEMISTRY

www.rsc.org/materialsA

Journal Name

RSCPublishing

ARTICLE

Rapid formation of superelastic 3D reduced graphene oxide networks with simultaneous removal of HI utilizing NIR irradiation

Cite this: DOI: 10.1039/x0xx00000x

Received ooth January 2012,
Accepted ooth January 2012

DOI: 10.1039/x0xx00000x

www.rsc.org/

Qiuwei Shi,[a] Chengyi Hou,[a] Hongzhi Wang,*[a] Qinghong Zhang[b] and Yaogang Li*[b]

Graphene foam with three-dimensional (3D) networks was formed following removal of the undesirable toxic iodide induced in HI reduced GO film through NIR light irradiation via a near infrared (NIR) light irradiation method at ambient laboratory conditions. Compact reduced graphene oxide films were used as the precursors which were fabricated through a vacuum filtration and HI reduction. A series of graphene foam which have alterable pore sizes ranging from a few to hundred micrometers rapidly formed under NIR light irradiation at different power density. The graphene foam has an ultimate tensile strength of about 15.3 MPa and could be compressed at a very large strain (ε = 60%) for 200 cycles without significant plastic deformation or degradation in compressive strength. This 3D graphene network is hydrophobic and showed high absorbing abilities for organic liquids. The adsorbed oil weight is up to about 27 times of graphene foam's weight after being immersed in oil-water mixture for two minutes, and 87.2% of adsorbed oil could be squeezed out and recycled. This process is highly repeatable, which makes our product a potential candidate for remove and recycle oil for environmental protection.

Introduction

Graphene and its three-dimensional (3D) constructions have been widely used in various fields of research due to its outstanding characteristics.[1-5] Production of graphene-based materials can be very high using redox method.[6-11] In addition, graphene oxide (GO) is a low cost building block for fabrication of high-performance macroscopic graphene-based materials.[6,12-16] Therefore, the redox strategy is considered to be a promising way to turn graphene applications into reality. In such a method, the hydriodic acid (HI) is recognized as one of the most effective and low-cost reduction agent for chemical reduction of graphene oxide.[6,8,17] However, the HI reduction process involves the use of very toxic and hazardous iodide which was risky to human health and the environment with long lasting effects.[18] In addition, the undesirable incorporation of iodide from the hydriodic acid into graphene sheets significantly alters the properties of the as-reduced graphene materials.[6-8] Although electrochemical reduction and thermal treatment methods have been introduced without such toxic reagents,[19,20] but these methods are time-consuming and the yield of graphene is very low.[13,19,21]

For comparison, light-induced reduction, as a mild and facile method, is now receiving attention as an alternative approach for producing graphene.[4,22-25] We have shown that large-area and high-crystallinity reduced graphene oxide film can be facilely fabricated with light irradiation (e.g., Xe lamp) at room temperature.[4] In addition, graphene's optoelectronic properties ensure a strong ($\pi\alpha$ = 2.3%), constant absorption of light across a wide range of wavelengths,[26] which could shed light on photothermal processes in graphene.[27] It is found that light irradiation could raise the temperature rapidly and significantly of both nano-sized and even 3D macroscopic graphene materials according to our previous reports.[28,29] Moreover, the thermal energy generated on graphene could be controlled in an environmentally friendly range (e.g., maximum temperature < 60 ºC) but still suitable for many applications.[29,30] Further considering of thermal decomposition of hydroiodic acid,[31] we surmised that the gentle thermal energy could break the forces of attraction between iodide and graphene those exist in the HI reduced graphene-based materials if photoreduction is conducted following HI chemical reduction of graphene oxide.

In this work, we demonstrated that the undesirable toxic iodide induced in graphene film with HI reduction can be readily removed through NIR light irradiation, and surprisingly, it was found that strong and superelastic graphene networks formed concurrently. Importantly, the light-assisted method allows us to alter the microstructure of macroscopic graphene materials. A series of production can be easily obtained for various applications. As a proof-of-concept, a hydrophobic and compressive graphene foams with uniform structure were prepared, which provides a new alternative for the cleanup and recycling of oil spills.

Results and discussion

Fig. 1a schematically shows the experimental procedure. In a typical experiment, the graphene oxide film (GOF) was firstly prepared through the vacuum filtered method,[8,32,33] which is an effective way to assemble GO sheets into compacted layer structure. Then, the hydrophilic GOF was transformed into the hydrophobic reduced graphene film (rGOF) by using hydriodic acid as the reduction reagent. rGOF could automatically separate from mixed cellulose ester membrane. Finally, the NIR light was used to irradiate the rGOF to fabricate 3D porous graphene foam (GF). The dramatic structure change of GF from rGOF can be clearly seen from scanning electron microscopy (SEM) images (insert). The thickness of GF was measured as up to 1.419 mm (Fig. 1b) while the thickness of rGOF is only about 20 μm. The freestanding GF has a metallic luster (Fig. 1c) after being irradiated by NIR light. The conductivity of GF measured through the four-probe method reached 1650.2 S/m, which is much higher than that of rGOF (583.5 S/m), representing one of the positive effects of NIR treatment. The freestanding GF are also highly flexible as shown in Fig. 1d.

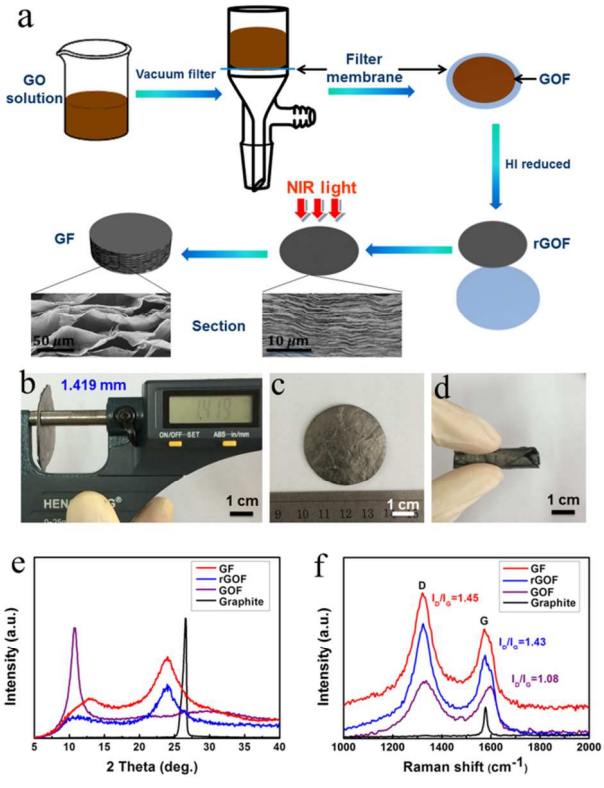

Fig. 1 (a) Schematic illustration for the NIR light irradiation-assisted process to fabricate GF. Insert SEM images show sectional morphology of rGOF and GF. (b) Thickness measurement of GF. (c and d) Photos show freestanding and flexible GF. (e) XRD patterns of the GF**1**, rGOF, GOF and graphite. (f) Raman spectra show the characteristic D and G bands of GF**1**, rGOF, GOF and graphite.

Different spectroscopy measurements were used to confirm the formation of rGO in the GF. Fig. 1e shows the X-ray diffraction (XRD) patterns of the initial precursor, intermediate and final products. The interlayer distance of the rGOF and GF were measured as 0.37 and 0.36 nm, respectively. These values are much lower than that of GOF (0.82 nm), but higher than that of graphite (0.34 nm). This is due to the iodine doping in rGOF and GF since the atomic radius of I (140 pm) is much bigger than that of C (70 pm).[8] In this work, the compact structured GOF has obvious differences with porous structured GOF in our early work.[8] HI is much more difficult to enter into its compact structure. Therefore there are small amount of residual graphene oxide in the final products, which are represented in XRD patterns as the small peaks around at 2θ = 11.0° and 12.8° for rGOF and GF. In addition, the shift of the peak indicates that the reduced graphene oxide in rGOF were further reduced by NIR light irradiation.[22] The Raman spectra in Fig. 1f show the characteristic D and G band of the obtained samples, which are in-plane E_{2g} vibrational mode and A_{1g} breat

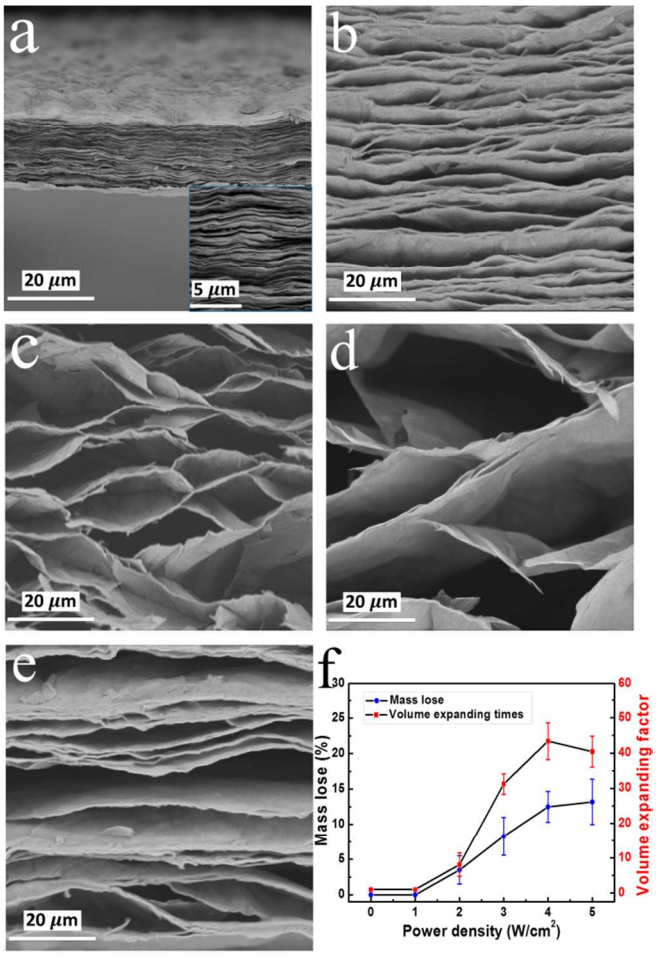

Fig. 2 Cross-sectional SEM images of rGOF (a) and GF after 5 s NIR treatment with different power densities: 2 W/cm^2 (b), 3 W/cm^2 (c), 4 W/cm^2 (d) and 5 W/cm^2 (e), scale bars are 20 μm. (f) The volume expansion and mass loss of GF foams as a function of the power density of NIR light.

hing mode,[15] respectively. The intensity ratio for the D and G bands (I_D/I_G) changes from 1.08 (GOF) to 1.43 (rGOF), and further increased to 1.45 (GF) after additional NIR light

treatment. This indicates that both chemical reduction and light reduction introduce defects on reduced graphene oxide.

Of particular interest is that NIR irradiation also simultaneously induced the pre-assembled rGO sheets in rGOF to be re-constructed in a 3D fashion. Fig. 2 shows the cross-sectional SEM images of the rGOF and GF. The compact layer structure of rGOF can be observed in Fig. 2a. Under NIR light irradiation, it can rapidly (within 5 s) transform to 3D porous structure. When power density of NIR light is 2 W/cm^2, the corresponding pore size, or interlayer distances between pore walls are about 10 μm (Fig. 2b). With increasing the power density to 3 and 4 W/cm^2, the pore size of GF significantly increased about 5 and 10 times (Fig. 2c and d), respectively. The GF exhibits a tunable 3D network structure with interconnected pores ranging from few to hundred micrometers. When the power density of the NIR light was increased to 5 W/cm^2, the pores were further opened and finally a channel-like structure was obtained (Fig. 2e). Volume expansion and mass loss of rGOF during above process were investigated detailedly (Fig. 2f). They are strongly dependent on the power density of NIR light, but barely change when the power density beyond 5 W/cm^2, indicating that the channel-like morphology would be the final state for the GF. Overall, altering morphologies and pore sizes of GF can be easily realized by controlling the power density of applied NIR light, which is superior to other methods for fabricating porous graphene foams.[5,34,35]

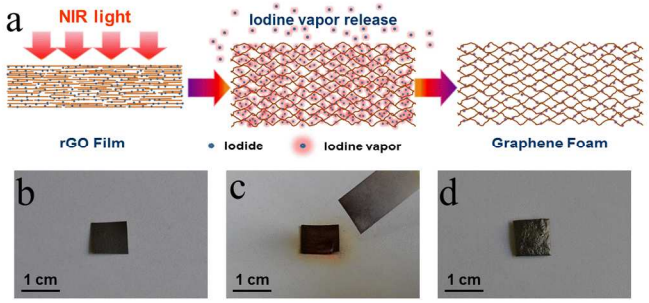

Fig. 3 (a) Schematic drawings illustrating iodine vapor-assisted pore-forming mechanism in GF. Photographs of rGOF (b), testing of iodine vapor release with starch iodide paper (c) and GF (d).

Fig. 3 schematically shows the formation process of porous GF. During the HI reduction of rGOF, a certain amount of iodide penetrated into interlayer of the rGOF. It is hardly washed out of the structure, as shown later in the text. However, under NIR irradiation, considerable amount of energy was generated and the temperature of rGOF remarkably increased up to 100–200 ºC within a few seconds (Fig. 4a). The thermal energy broke the forces of attraction between iodide and graphene, meanwhile the iodide was reduced into iodine (Fig. 6) and further formed iodine vapor (iodine sublimation temperature: 45 ºC). Fig. 4b and c and Supplementary video1 and 2 clearly show that the purple iodine vapor was released along with rapid expansion of GF volume, and the released iodine vapor rendered starch iodide paper blue. Moreover, the GF was further reduced during this process, according to the XRD, Raman, and X-ray photoelectron spectroscopy (XPS) results shown below.

We further investigated the influence of NIR irradiation time on the structure of rGOF. Fig. 4a shows the surface temperature curve of rGOF under continuous NIR light irradiation. The average temperature measured at the region indicated in the

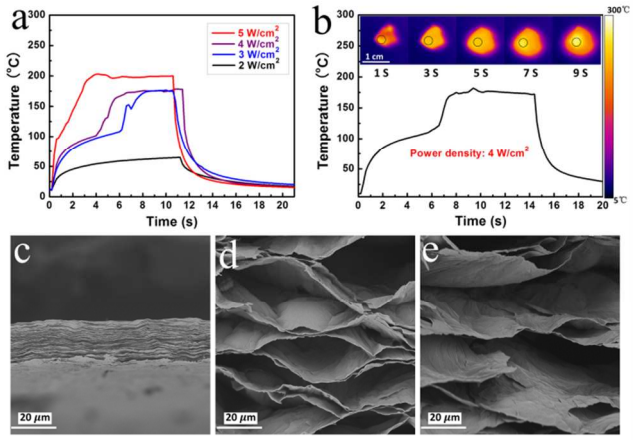

Fig. 4 (a) Temperature curve for rGOF when exposed to NIR light at different power densities. (b) Temperature curve for rGOF exposed to 4 W/cm^2 NIR light, insets show their infrared thermal images. Cross-sectional SEM images of GF irradiated by 4 W/cm^2 NIR light for: 1 s (c), 5 s (d), 9 s (e).

infrared thermal images increased remarkably within 10 seconds. It is notable that the surface temperature changed in two steps. Typically, as shown in Fig. 4b and Supplementary video 3 (infrared thermal video showing the change of temperature visually), the measured mean surface temperature of rGOF increased to and maintained at around 100 ºC (from 2 to 6 s) under 4 W/cm^2 NIR light irradiation, and further increased to and maintained at about 175 ºC after 7 s irradiation until turning off the NIR light. Therefore, we characterized its structure at the beginning, first step (2–6 s), and second step (6–14 s) of temperature change. Three different results were observed. Fig. 4c, d and e show typical cross-sectional SEM images of rGOF after being irradiated by NIR light (power density: 4 W/cm^2) for 1, 5 and 9 s, respectively. A much more uniform porous structure could be found in Fig. 4d, indicating a suitable reaction condition. This sample (labeled as GF**1**) with such ideal structure would be a promising candidate for various applications. The others with barely or irregularly opened pores would also be useful in many specific area such as nano filtration and particle size selection.

Above results suggest that when reducing rGOF, the light-induced release of iodine contributes most to the formation of a foamed structure. To accurately understand the present results, we next performed detailed characterization of the samples. The distribution of iodine in the rGOF and GF**1** was analyzed by energy dispersive spectrometer (EDS) mapping. Fig. 5a and b show the EDS mapping images of signals from C (red), O (blue), and I (purple) element measured on rGOF' surface and GF**1**' inner porous surface. All elemental analyzes were

repeated three times and presented after normalization. As shown in Fig. 5a and b, the distribution of iodine (purple) in the rGOF and GF**1** is homogenized. Semaphore feedback from iodine (purple) can be drawn that iodine in the GF**1** was significantly less than the iodine in the rGOF. The elemental mass percentage of iodine in the rGOF and GF**1** were 18.63% and 5.16%, respectively (Fig. 5c). A very considerable amount of iodine was released in the process of NIR light irradiation.

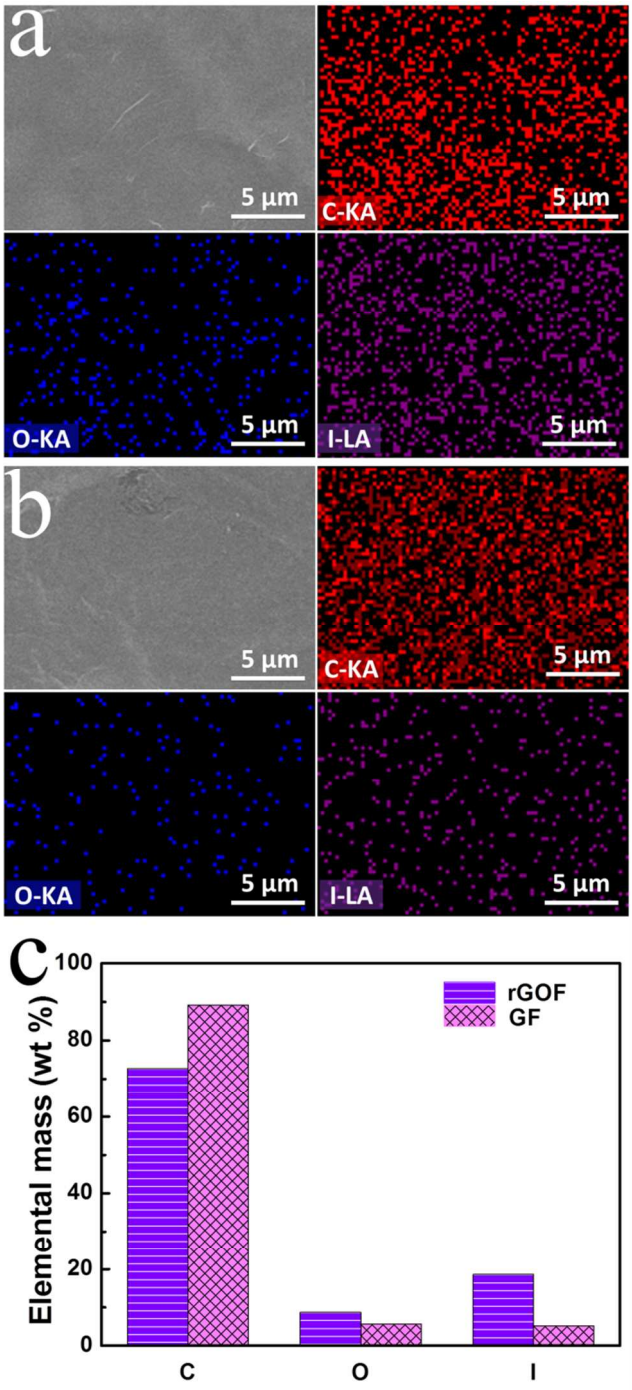

Fig. 5 EDS mapping images of signals from C, O, and I element for rGOF' surface (a) and GF**1**' inner porous surface (b). Elemental mass percentage of C, O, and I element for rGOF and GF**1** (c).

XPS was also performed perpendicularly to the surface in order to investigate surface properties of the samples at various steps of preparation. As shown in Fig. 6a, the detected peaks at 284.6, 532.2, and around 625 eV are corresponding to the characteristic of C1s, O1s, I3d spectrums, respectively. The weak peaks around at 620.0 and 631.0 eV were corresponding to small amounts of elemental iodine and iodide ions, respectively.[36] The high resolution spectrum shows the deconvoluted result of C1s of GOF, rGOF and GF**1**. In the spectrum (Fig. 6b–d), four peaks centering at 284.7 eV (C=C/C-C),[37] 286.7 eV (C-O-C),[38] 287.3 eV (C=O),[39,40] and 289.1 eV (O=C-OH) are found in Fig. 6b;[41,42] Peaks centering at 284.6 eV (C=C/C-C),[42,43] 286.4 eV (C-O-C, C-OH),[41] 287.2 eV (C=O),[40,41] and 289.1 eV (O=C-OH) are found in Fig. 6c;[41,42] Peaks centering at 284.6 eV (C=C/C-C),[42,43] 286.4 eV (C-O-C, C-OH),[41] 287.6 eV (C=O),[42] and 289.1 eV (O=C-OH) are found in Fig. 6d.[41,42] Curve fitting results of C1s spectrum are shown in Table 1. It is obvious that the ratio of oxygen-containing functional groups is decreasing with the duration of HI and NIR treatment. The characteristic peaks of elemental iodine and iodide ions in rGOF and GF**1** can be deconvoluted into two types of I chemical state (Fig. 6e and f). The peaks centered at 619.9 (Fig. 6e) and 620.0 (Fig. 6f) eV are assigned to I elemental.[36] The negative monovalent I^{-1} (around 630 eV)

Table 1 Curve fitting results of XPS C1s spectrum.

	peak	BE[a] (eV)	FWHM[b] (eV)	%
GOF	C=C/C-C	284.7	1.5	51.4
	C-O-C	286.7	1.1	27.2
	C=O	287.3	1.0	14.8
	O=C-OH	289.1	2.4	6.6
rGOF	C=C/C-C	284.6	1.2	75.8
	C-O-C, C-OH	286.4	1.5	9.7
	C=O	287.2	2.4	9.1
	COOH	289.1	1.5	5.4
GF**1**	C=C/C-C	284.6	1.2	78.9
	C-O-C, C-OH	286.4	1.7	9.1
	C=O	287.6	1.5	7.2
	COOH	289.1	1.4	4.8

[a] Binding energy, [b] Full width at half-maximum

Table 2 The content (at %) of C, O and I elementary of GOF, rGOF and GF**1**.

	Spectrum	At. (%)
GOF	C1s	74.55
	O1s	25.45
	I3d	–
rGOF	C1s	81.72
	O1s	17.38
	I3d	0.90
GF**1**	C1s	83.17
	O1s	16.54
	I3d	0.29

represents hydriodic acid. The presence of iodine elemental was caused by the reduction of iodide ions. The content (at. %) of C, O and I elementary of GOF, rGOF and GF**1** are summarized in Table 2. It is observed that, the C/O ratio for GOF is 2.9, after HI reduction and further reduction with NIR light, which increase to 4.7 for rGOF and 5.0 GF1.The increase of C/O ratio indicating the reduction effect of NIR light.[42-44] The results not only confirm the reduction effect of NIR light, but also identify the release of iodine (the I/I^{-1} ratio for rGOF and GF**1**, which was calculated based on the peak areas, decreases from 1.66 to 1.37). Overall, the above spectroscopy results strongly support our proposed GF formation mechanism.

Owing to the uniform porous structure of GF**1**, the compression tests (ε = 60%) revealed that the as-formed GF**1** with a calculated density of about 0.07 g/cm^3 exhibited excellent mechanical properties (Fig. 7). As shown in Fig. 7a, the GF**1** is gradually compressed and densified in the loading process. In the unloading process, compressive stress decreased

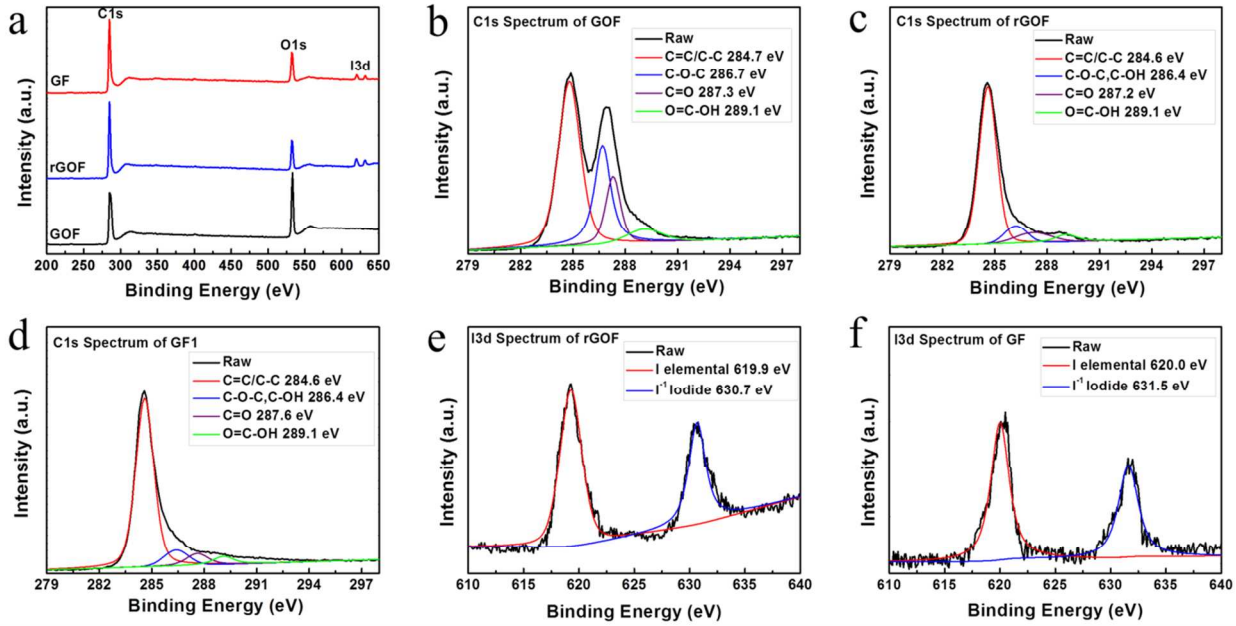

Fig. 6 (a) X-ray photoelectron spectra of GOF, rGOF and GF**1**. High resolution C1s spectrum of GOF (b), rGOF (c) and GF**1** (d). High resolution I3d spectrum of rGOF (e) and GF**1** (f).

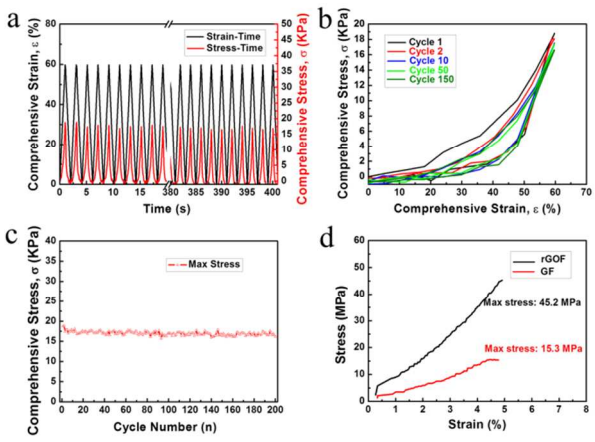

Fig. 7 Multi-cycle compressive properties and tensile strength of the elastic GF**1** with a density of 0.07 g/cm^3. (a) The fatigue tests (a-c, ε = 60%, f = 0.5 Hz) with strain-stress-time curve to 200 cycles of the elastic GF**1**. (b) Hysteresis studies for the 1, 2, 10, 50 and 150 loading-unloading cycles of the elastic GF**1**. (c) Max stresses for 200 cycles of the elastic GF**1**. (d) The tensile strength with stress-strain curves of the rGOF (black) and GF**1** (red).

along with restoring of GF timely. The structure can rapidly and completely recover to the original state within ca. 1 s. The highly elastic graphene foam also exhibited excellent cycling performance. A hysteresis cyclic compression test (ε = 60%) is shown in Fig. 7b, the degradation of maximum compressive strength is approximately 10.8% after 150 cycles. The integrating energy of loading and unloading process indicates that 70.3% of the energy is retained during compression. The energy dissipation is largely caused by the friction between graphene sheets and movement of air through the porous GF.[45] The maximum stress decreases 7.3% in the first 2 cycles (from 18.79 to 17.42 KPa) and then stabilizes at 17 KPa in the subsequent cycles shown in Fig. 7c, which is more stable than graphene elastomer synthesized by freeze casting method.[46] The measured tensile strength of GF**1** and rGOF are up to 15.3 (red line) and 45.3 (black line) MPa, respectively (Fig. 7d). The tensile strain of GF**1** and rGOF is 4.9% and 4.7%, respectively. The strength of porous GF**1** is lower than the strength of compact rGOF, this is because that the friction between graphene sheets of porous structure is less than a compact structure. The tensile strength of our porous graphene foam

material is 5 times larger than that of other reduced graphene oxide foams prepared by a leavening strategy.[13]

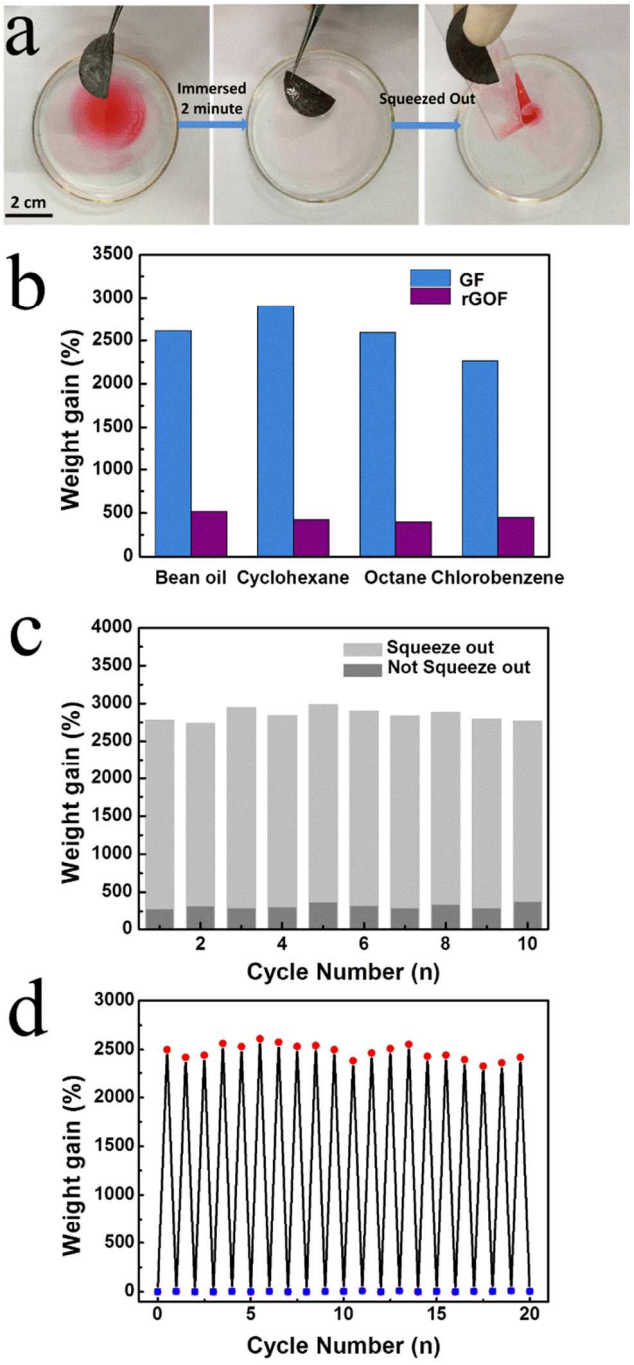

Fig. 8 Oil adsorption capacities studies of the porous GF**1**. (a) Photographs show the bean oil can be removed by freestanding GF**1** and squeeze out when compressed (bean oil was labeled with Oil red dye). (b) Absorption capacities compared of the GF**1** and rGOF for a selection of organic solvents and oils. (c) Absorption capacity and percentage of recycled for bean oil of the elastic GF**1**. (d) The GF absorption recyclability of bean oil over 20 cycles (squares: the restored weight of GF**1** after washing with hexane, dots: the weight gain after saturated adsorption of bean oil).

The advantages of having a superelastic and mechanically strong structure can be further demonstrated by application test. As a proof-of-concept, oil cleanup and recycling performance of GF**1** was investigated. The GF**1** is highly hydrophobic (the contact angle is about 110º), possessing super-high absorption capacities and ultrafast absorption rate for oil and organic solvents. Fig. 8a shows that the oil can be removed from oil-water mixture by freestanding elastic GF**1** in two minutes, which are faster than the results reported in other work (5 minutes).[47] As shown in Fig. 8b, weight gain was used to represent the absorption capacities of the GF**1** and rGOF for bean oil and other organic solvents.[13,48,49] The rGOF adsorption amount of bean oil and other organic solvents are approximately 5 times and 4 times of its own weight respectively. The weight gain of GF**1** is up to about 27 times of its own weight for bean oil and organic solvents, absorption capacities of GF**1** were higher than the compact rGOF and the superwetting inorganic nanowire membranes.[49] Most importantly, adsorbed oil could be recycled due to the excellentelastic properties of GF**1**. Fig. 8c shows the proportion of the squeezed out bean oil from the saturated adsorb GF**1**. After 10 adsorption-squeezing cycles, the measured mean recycling proportion is up to 87.2%. As shown in Fig. 8d, the weight gain of GF**1** maintained at as high as 26 times of its own weight after 20 cycles. Therefore, the superelastic GF**1** can tolerate repeatable oil recycling under squeezing. This experiment demonstrate the potential of GFs for practical applications such as oil spill cleanup.

Experimental

Materials

Graphite powder (500 meshes, purity: 99%) was purchased from Shanghai Yifan Graphite Co. Ltd (China). Bean oil was purchased from Shanghai Liangyou Haishi Oils&Fats Industrial Co. Ltd (China). Oil Red was purchased from Sigma-Aldrich Chemical Co. Inc (United States). Mixed cellulose ester membrane (pore diameter: 0.22 μm) was purchased from the Peninsula Shanghai Industrial Co. Ltd (China). Starch iodide paper was purchased from Shanghai SSS reagent Co. Ltd (China). Potassium permanganate, sulfuric acid, hydrogen peroxide (30 vol%), hydrochloric acid, hydriodic acid, cyclohexane, octane and chlorobenzene were purchased from Sinopharm Chemical Reagent Co. Ltd (China). All reagents were analytical grade and used without further treatment.

Synthesis of GO

Graphite oxide was prepared by oxidation of flake graphite according to the modified Hummers' method.[50,51] Flake graphite powder (2 g) was added to concentrated sulfuric acid (46 mL, 0 ºC) under stirring in an ice bath. Then, potassium permanganate (6 g) was added gradually with stirring. Successively, the mixture was stirred at 35 ºC for 2 h. Then, distilled water (92 mL) was slowly added to the mixture with the temperature rise from 35 ºC to 98 ºC, and the mixture was maintained at 98 ºC for 15 minutes. After that, the mixture was added to the preheated hydrogen peroxide solution (30%, 280

mL). Finally, the mixture was filtered and washed with hydrochloric acid aqueous solution (10 vol%, 500 mL) to remove metal ions. The yellow brown powder of GO is obtained after dried and grinded.

Synthesis of graphene networks

GO film (GOF) was first prepared through vacuum filtration of GO aqueous dispersion. Then it was chemical reduced by using HI reduction method according to previous reports.[8,17] The as-obtained reduced graphene oxide film (rGOF) was thoroughly washed with water and dried at room temperature. Then it was further irradiated under an NIR light (power density: 2, 3, 4 and 5 W/cm^2) to fabricate 3D porous graphene foam (GF).

Adsorption capacity of GF

For oil and organic solvents sorption tests, bean oil and organic solvents sorption (cyclohexane, octane and chlorobenzene) were labeled with oil red for being more figurative. Then the labeled hydrophobicity solvents were poured onto a water surface in a petri dish. The GF was weighed and put onto the surface of the water-oil mixtures. Then the hydrophobicity solvents were adsorbed into the open porous structure of GF. After 2 minutes, it reaches saturated adsorption and weighed. The sorption capability (weight gain) of GF was accord to the ASTMF726-99 (Standard Test Method for Sorbent Performance of adsorbents).[47] The sorption capability (weight gain) of the GF was represented using the following equation:

$$\text{Weight gain}\ (\%) = \frac{W_t - W_0}{W_0} \times 100 \qquad (1)$$

where W_0 was the original dry weight of the porous structured GF and W_t was the weight of the GF with saturated adsorption of hydrophobicity solvents. All experiments were operated at room temperature and conducted three times, and calculated the average value substituted into the equation. Weight measurements were done rapidly to prevent evaporation of the hydrophobicity solvents.

Characterization and Measurements

The light source was an external near infrared semiconductor light device ADR 1805 (Shang Hai SFOLT Co. Ltd, China) whose power could be adjusted continuously (0–2 W). The morphologies of the as-prepared samples were characterized by Phenom G2 Pro Scanning electron microscopy (SEM) at 10.0 kV. The infrared thermal images and time versus temperature profiles were measured using a FLIR ThermoVision A40m infrared thermometer. Energy dispersive spectrometer mapping of each element was obtained using a JSM-6700F FESEM equipped with an Oxford Instruments EDS detector. The specific surface area of the graphene foam was tested using physical adsorption of N_2 at liquid-nitrogen temperature on an automatic volumetric sorption analyzer ASAP 2020. The X-ray diffraction (XRD) spectroscopy was performed on a Rigaku D/MAX 2550 V X-ray diffractometer with Cu K_α irradiation (λ = 1.5406 Å) with a step size of 0.01°. The operating voltage and current was 40 kV and 300mA. Raman spectra were carried out on a Renishaw in plus laser Raman spectrometer with λ_{exc} = 633 nm. Compression cycle experiments of as-prepared products were conducted with a digital micrometer and an Instron universal material testing system (INSTRON 5969). The photographs were taken with a charge coupled device (CCD) video camera PowerShot G10, Canon. X-ray photoelectron spectroscopy measurements were characterized with an SECA Lab 220i-XL spectrometer by using an unmonochromated Al K_α (1486.6 eV) X-ray source.

Conclusions

In conclusion, we have demonstrated that superelastic 3D porous reduced graphene oxide foam can be made rapidly by NIR light irradiating based on traditional HI reduced graphene oxide film. Various 3D graphene networks with different pore sizes can be obtained by controlling the power density of the NIR light. The 3D network formation mechanism was understood as light-induced release of iodine. Therefore, our strategy successfully reduces the environmental harm of the widely used HI-reduced graphene materials, makes it attractive in a wide variety of applications such as oil absorption. On the other hand, it also open up new opportunities to prepare novel 3D networks from other 2D nanomaterials.

Acknowledgements

We gratefully acknowledge the financial support by NSF of China (No. 51172042), MOE of China (IRT1221, No.111-2-04), STC of Shanghai (12nm0503900, 13JC1400200), SRFDP (20110075130001), and the Fundamental Research Funds for the Central Universities.

Notes and references

[a] State Key Laboratory for Modification of Chemical Fibers and Polymer Materials, College of Materials Science and Engineering, Donghua University, Shanghai 201620, P. R. China. E-mail: wanghz@dhu.edu.cn; Fax: +86-021-67792855; Tel: +86-021-67792881

[b] Engineering Research Center of Advanced Glasses Manufacturing Technology, Ministry of Education, College of Materials Science and Engineering, Donghua University, Shanghai 201620, P. R. China. E-mail: yaogang_li@dhu.edu.cn; Fax: +86-021-67792855; Tel: +86-021-67792526

† Electronic Supplementary Information (ESI) available: [details of any supplementary information available should be included here]. See DOI: 10.1039/b000000x/

1. C. Berger, Z. M. Song, X. B. Li, X. S. Wu, N. Brown, C. Naud, D. Mayou, T. B. Li, J. Hass, A. N. Marchenkov, E. H. Conrad, P. N. First and W. A. de Heer, *Science*, 2006, **312**, 1191.
2. M. I. Katsnelson, *Mater. Today.*, 2007, **10**, 20.
3. F. Scarpa, S. Adhikari and A. S. Phani, *Nanotechnology*, 2009, **20**.
4. Y. L. Shao, H. Z. Wang, Q. H. Zhang and Y. G. Li, *NPG Asia Mater.*, 2014, **6**.

5. Y. X. Xu, K. X. Sheng, C. Li and G. Q. Shi, *ACS Nano*, 2010, **4**, 4324.
6. J. Kim, J. H. Jeon, H. J. Kim, H. Lim and I. K. Oh, *ACS Nano*, 2014, **8**, 2986.
7. G. J. Huang, C. Y. Hou, Y. L. Shao, H. Z. Wang, Q. H. Zhang, Y. G. Li and M. F. Zhu, *Sci Rep. UK*, 2014, **4**.
8. C. Y. Hou, H. Z. Wang, Q. H. Zhang, Y. G. Li and M. F. Zhu, *Adv. Mater.*, 2014, **26**, 5018.
9. P. Song, X. Y. Zhang, M. X. Sun, X. L. Cui and Y. H. Lin, *RSC Adv.*, 2012, **2**, 1168.
10. S. Stankovich, D. A. Dikin, R. D. Piner, K. A. Kohlhaas, A. Kleinhammes, Y. Jia, Y. Wu, S. T. Nguyen and R. S. Ruoff, *Carbon*, 2007, **45**, 1558.
11. H. J. Shin, K. K. Kim, A. Benayad, S. M. Yoon, H. K. Park, I. S. Jung, M. H. Jin, H. K. Jeong, J. M. Kim, J. Y. Choi and Y. H. Lee, *Adv. Funct. Mater.*, 2009, **19**, 1987.
12. H. H. Cheng, C. G. Hu, Y. Zhao and L. T. Qu, *NPG Asia Mater.*, 2014, **6**.
13. Z. Q. Niu, J. Chen, H. H. Hng, J. Ma and X. D. Chen, *Adv. Mater.*, 2012, **24**, 4144.
14. C. Y. Hou, Q. H. Zhang, Y. G. Li and H. Z. Wang, *J. Hazard Mater.*, 2012, **205**, 229.
15. C. Y. Hou, T. Huang, H. Z. Wang, H. Yu, Q. H. Zhang and Y. G. Li, *Sci. Rep. UK*, 2013, **3**.
16. C. Y. Hou, Q. H. Zhang, Y. G. Li and H. Z. Wang, *Carbon*, 2012, **50**, 1959.
17. I. K. Moon, J. Lee, R. S. Ruoff and H. Lee, *Nat. Commun.*, 2010, **1**.
18. G. Lionelli, E. Pickus, J. Bray, W. Lawrence Jr and R. Korentager, *J. Burn Care Res.*, 2001, **22**, 341.
19. G. K. Ramesha and S. Sampath, *J. Phys. Chem. C*, 2009, **113**, 7985.
20. H. L. Guo, X. F. Wang, Q. Y. Qian, F. B. Wang and X. H. Xia, *ACS Nano*, 2009, **3**, 2653.
21. Y. W. Zhu, M. D. Stoller, W. W. Cai, A. Velamakanni, R. D. Piner, D. Chen and R. S. Ruoff, *ACS Nano*, 2010, **4**, 1227.
22. Y. L. Zhang, L. Guo, H. Xia, Q. D. Chen, J. Feng and H. B. Sun, *Adv. Opt. Mater.*, 2014, **2**, 10.
23. Y. L. Shao, H. Z. Wang, Q. H. Zhang and Y. G. Li, *J. Mater. Chem. C*, 2013, **1**, 1245.
24. M. Koinuma, C. Ogata, Y. Kamei, K. Hatakeyama, H. Tateishi, Y. Watanabe, T. Taniguchi, K. Gezuhara, S. Hayami, A. Funatsu, M. Sakata, Y. Kuwahara, S. Kurihara and Y. Matsumoto, *J. Phys. Chem. C*, 2012, **116**, 19822.
25. Y. Matsumoto, M. Koinuma, S. Y. Kim, Y. Watanabe, T. Taniguchi, K. Hatakeyama, H. Tateishi and S. Ida, *ACS Appl. Mater. Inter.*, 2010, **2**, 3461.
26. R. A. Barton, I. R. Storch, V. P. Adiga, R. Sakakibara, B. R. Cipriany, B. Ilic, S. P. Wang, P. Ong, P. L. McEuen, J. M. Parpia and H. G. Craighead, *Nano Lett.*, 2012, **12**, 4681.
27. N. M. Gabor, J. C. W. Song, Q. Ma, N. L. Nair, T. Taychatanapat, K. Watanabe, T. Taniguchi, L. S. Levitov and P. Jarillo-Herrero, *Science*, 2011, **334**, 648.
28. C. Y. Hou, H. C. Quan, Y. R. Duan, Q. H. Zhang, H. Z. Wang and Y. G. Li, *Nanoscale*, 2013, **5**, 1227.
29. C. Y. Hou, Y. R. Duan, Q. H. Zhang, H. Z. Wang and Y. G. Li, *J. Mater. Chem.*, 2012, **22**, 14991.
30. J. T. Robinson, S. M. Tabakman, Y. Y. Liang, H. L. Wang, H. S. Casalongue, D. Vinh and H. J. Dai, *J. Am. Chem. Soc.*, 2011, **133**, 6825.
31. W. J. Husa and P. S. Shattuck, *J. Am. Pharm. Assoc.*, 1932, **21**, 114.
32. H. B. Huang, Z. G. Song, N. Wei, L. Shi, Y. Y. Mao, Y. L. Ying, L. W. Sun, Z. P. Xu and X. S. Peng, *Nat. Commun.*, 2013, **4**.
33. B. S. Kong, J. X. Geng and H. T. Jung, *Chem. Commun.*, 2009, 2174.
34. Y. Zhao, C. G. Hu, Y. Hu, H. H. Cheng, G. Q. Shi and L. T. Qu, *Angew. Chem. Int. Ed.*, 2012, **51**, 11371.
35. A. H. Lu, G. P. Hao and Q. Sun, *Angew. Chem. Int. Ed.*, 2013, **52**, 7930.
36. R. D. Seals, R. Alexander, L. T. Taylor and J. G. Dillard, *Inorg. Chem.*, 1973, **12**, 2485.
37. F. Xiang, J. Zhong, N. Y. Gu, R. Mukherjee, I. K. Oh, N. Koratkar and Z. Y. Yang, *Carbon*, 2014, **75**, 201.
38. H. Ham, T. V. Khai, N. H. Park, D. S. So, J. W. Lee, H. G. Na, Y. J. Kwon, H. Y. Cho and H. W. Kim, *Nanotechnology*, 2014, **25**.
39. H. Chen, D. D. Shao, J. X. Li and X. K. Wang, *Chem. Eng. J.*, 2014, **254**, 623.
40. N. Zhao, X.-N. Cheng, J. Yang, M.-X. Yang, S.-H. Zheng and Y.-Z. Zhou, *J. Phys. Chem. Solids*, 2014, **75**, 1141.
41. A. K. Das, M. Srivastav, R. K. Layek, M. E. Uddin, D. Jung, N. H. Kim and J. H. Lee, *J. Mater. Chem. A*, 2014, **2**, 1332.
42. Z. Bo, X. R. Shuai, S. Mao, H. C. Yang, J. J. Qian, J. H. Chen, J. H. Yan and K. Cen, *Sci Rep. UK*, 2014, **4**.
43. H. Hu, Z. B. Zhao, W. B. Wan, Y. Gogotsi and J. S. Qiu, *Adv. Mater.*, 2013, **25**, 2219.
44. F. Xiang, J. Zhong, N. Gu, R. Mukherjee, I.-K. Oh, N. Koratkar and Z. Yang, *Carbon*, 2014, **75**, 201.
45. A. Y. Cao, P. L. Dickrell, W. G. Sawyer, M. N. Ghasemi-Nejhad and P. M. Ajayan, *Science*, 2005, **310**, 1307.
46. L. Qiu, J. Z. Liu, S. L. Y. Chang, Y. Z. Wu and D. Li, *Nat. Commun.*, 2012, **3**.
47. H. Li, L. F. Liu and F. L. Yang, *J. Mater. Chem. A*, 2013, **1**, 3446.
48. H. C. Bi, X. Xie, K. B. Yin, Y. L. Zhou, S. Wan, R. S. Ruoff and L. T. Sun, *J. Mater. Chem. A*, 2014, **2**, 1652.
49. J. K. Yuan, X. G. Liu, O. Akbulut, J. Q. Hu, S. L. Suib, J. Kong and F. Stellacci, *Nat. Nanotechnol.*, 2008, **3**, 332.
50. W. S. Hummers and R. E. Offeman, *J. Am. Chem. Soc.*, 1958, **80**, 1339.
51. N. I. Kovtyukhova, P. J. Ollivier, B. R. Martin, T. E. Mallouk, S. A. Chizhik, E. V. Buzaneva and A. D. Gorchinskiy, *Chem. Mater.*, 1999, **11**, 771.